ACS OMEGA

http://pubs.acs.org/journal/acsodf

Article

Characteristics of Water-Soluble Inorganic Ions in $PM_{2.5}$ in Typical Urban Areas of Beijing, China

Xiuping Hong, Kang Yang,* Handong Liang,* and Yunyun Shi

Cite This: *ACS Omega* 2022, 7, 35575−35585

Read Online

ACCESS | Metrics & More | Article Recommendations

ABSTRACT: Following the implementation of "coal-to-gas conversion" policy in the Haidian District of Beijing during summer, the present comparative study was performed employing 41 $PM_{2.5}$ samples as precursors to analyze the characteristics of water-soluble inorganic ions. The concentrations of water-soluble inorganic ions in $PM_{2.5}$ were analyzed by ion chromatography, and the occurrence form of ions was characterized via time-of-flight secondary ion mass spectrometry (TOF-SIMS). Results revealed that the daily average mass concentration of $PM_{2.5}$ in Beijing during the sampling period was 94.28 ± 52.49 $\mu g/m^3$. As compared to the winter of 2016, the average daily $PM_{2.5}$ concentration in Beijing decreased by 29 $\mu g/m^3$ in 2017 (28.2% decrease), with a remarkable decline in the number of days with pollution. During the pollution period, the concentrations of NO_3^-, SO_4^{2-}, and NH_4^+ were significantly higher in $PM_{2.5}$ as compared to the cleaning period. The ratio of the concentrations of $[NO_3^-]/[SO_4^{2-}]$ was greater than 1, and the contribution from mobile sources was relatively large, indicating that the implementation of the "coal-to-gas conversion" policy in Beijing has led to the reduction of SO_4^{2-} emissions from fixed sources, such as coal. Furthermore, TOF-SIMS analysis results showed that NH_4^+ tended to exist in the form of molecular ammonium sulfate or ammonium hydrogen sulfate during the period of pollution.

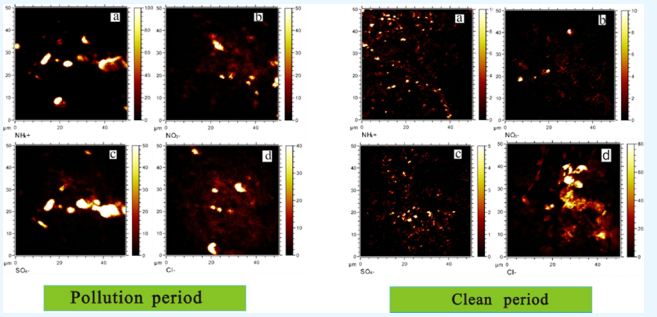

1. INTRODUCTION

Particulate matter ($PM_{2.5}$) comprises atmospheric particles with an aerodynamic diameter of less than 2.5 μm; they are fine atmospheric particles that can be deeply inhaled by humans, which is a common manifestation of air pollution.[1−4] Inorganic salts found in $PM_{2.5}$, such as those of water-soluble inorganic ions, including SO_4^{2-}, NO_3^{2-}, Cl^-, and NH_4^+, have the physicochemical of water absorption and condensation. Notably, they are known for initiating smog formation under specific meteorological conditions (relative humidity more than 60%).[5−7] SO_4^{2-}, NO_3^{2-}, and NH_4^+ (SNA) are the main inorganic ions in $PM_{2.5}$, accounting for 80% or more of all water-soluble ions.[8−10] The abundance of SNA is dependent on the relative abundance of the corresponding gaseous precursors, that is, NO_x, SO_2, and NH_3, and their atmospheric conversion rate, as well as several meteorological factors, including temperature and humidity.[11−13] Water-soluble inorganic ions have a higher ratio of the extinction coefficient in the atmosphere, which is the main cause for decreased visibility in many cities. They are also involved in the formation of a complex air pollution system.[14] Therefore, it is crucial to elucidate the characteristic pollution and occurrence of secondary water-soluble ions for an improved regulation of environmental pollution and human health safety.

There are numerous studies on the composition and formation of water-soluble inorganic ions. In detail, Xie et al.[15] reported that $PM_{2.5}$ mass was driven by NO_3^- during cold months (October−March) or SO_4^{2-} during warm months (September, April−August). Li et al.[16] found that the increase in the water-soluble inorganic ion concentration is one of the main causes of heavy pollution. Furthermore, Wu et al.[17] reported that the ratio of the concentrations of SNA to $PM_{2.5}$ is directly proportional to the pollution levels. According to field-based analysis by Huang et al.,[18] water-soluble inorganic ion concentrations, such as those of SNA, are predominates during the high-concentration maintenance phase of heavy pollution, and the concentration further increases during the static weather mode. However, currently, there is a lack of research on the binding morphology of water-soluble inorganic ions that are challenging to characterize. For example, the in situ single-particle analysis method using SEM/EDS can character-

Received: May 11, 2022
Accepted: September 16, 2022
Published: September 26, 2022

https://doi.org/10.1021/acsomega.2c02919
ACS Omega 2022, 7, 35575−35585

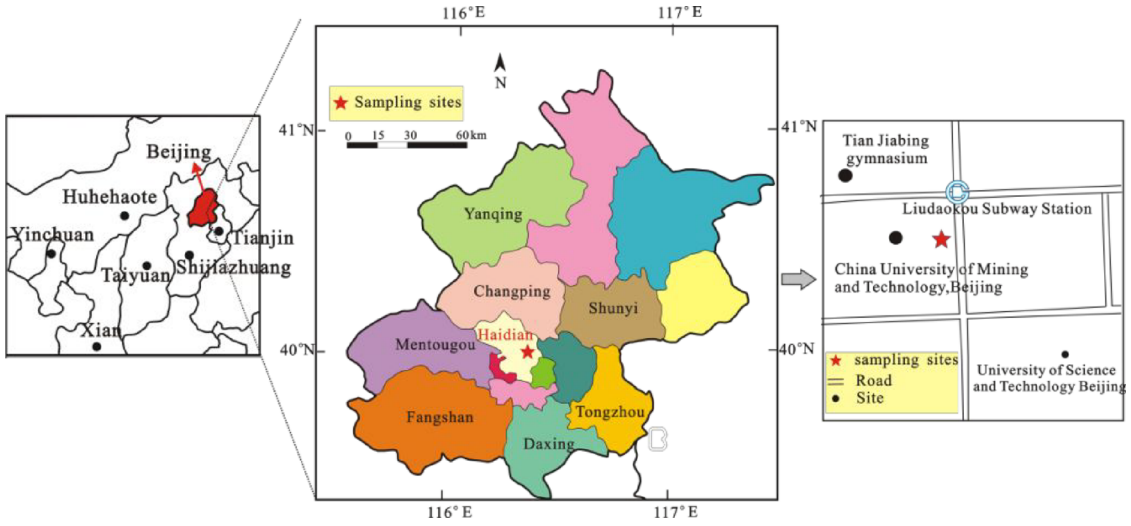

Figure 1. Schematic map of the sampling site.

ize chemical composition and morphology of various inorganic compounds and elements.[19,20] However, this analytical method cannot detect the SNA ions. Time-of-flight secondary ion mass spectrometry (TOF-SIMS) is a technique for surface in situ microanalysis.[21,22] In previous research, our team analyzed three samples of a typical heavy air pollution period collected from an urban area of Beijing in 2015 and found that more than 10 kinds of water-soluble inorganic ions including ammonium were detected by TOF-SIMS and the presence of ammonium bisulfate (NH_4HSO_4) single particles were also observed,[23] indicating the characteristics, advantage, and application potential of TOF-SIMS for the characterization of water-soluble inorganic components in $PM_{2.5}$. However, there are only three samples in the previous study, which may be under-represented. As an important political and economic region in China, there is an increasing developmental change in Beijing's energy structure among other factors that are detrimental and pose serious pressure on the region's environment. Since the beginning of the 21st century, increasing human activities have led to severe $PM_{2.5}$ pollution in Beijing, which is reflected in the overall increase in its mass concentration and the formation of haze during winter.[24,25] Interestingly, to tackle severe aerosol pollution, the Chinese State Council issued the "The Air Pollution Prevention and Control Action Plan" ("coal to gas" police) in September 2013, committed to reducing $PM_{2.5}$ concentrations, and promoted a series of control measures that were more stringent and ambitious than ever before, such as energy transforming from coal combustion into the use of natural gas and electricity, eliminating outdated coal-fired boilers, addressing automobile exhaust, managing heavy-duty diesel vehicles, developing alternative energy vehicles, and cleaning up outdated old vehicles.[26−30] From 2016 to 2017, "Beijing-Tianjin-Hebei Air Pollution Prevention and Control" pushed the coal-to-gas policy to a climax.[28] Benefiting from the Air Pollution Prevention and Control Action Plan, emissions of a major air pollutant have decreased by 59% for SO_2, 21% for NO_x, and 33% for PM2.5 from 2013 to 2017.[7,29] In the present study, we characterized $PM_{2.5}$ via TOF-SIMS. Furthermore, we analyzed the distribution characteristics of water-soluble inorganic ions in $PM_{2.5}$ and the generation of secondary ions during the winter season in Beijing after implementation of the policy.

2. EXPERIMENTS

2.1. Sample Collection. The $PM_{2.5}$ sampling took place at the roof top of the national building of China University of Mining and Technology (Beijing) in the Haidian District, Beijing (116°20′38.77″E, 39°59′45.98″N), which was approximately 18 m from the ground. There were no elevated buildings or industrial air pollution sources around the study site, and thus, the area reliably reflected the pollution characteristics of Beijing.

$PM_{2.5}$ samples were simultaneously collected on quartz filters (PALL Company, USA) with 90 mm diameter from December 18, 2017 to January 30, 2018. We used a median volume sampler along with $PM_{2.5}$ cutting equipment (manufactured by Laoying, Qingdao, China) at a flow rate of 100 L min^{-1}, and each sampling event lasted for 24 h (from 8:00 a.m. to next 8:00 a.m.). A total of 41 valid samples were collected. To remove volatile substances and other impurities, the membranes were baked at 450 °C for 12 h prior to sampling. Moreover, the filters were weighed under controlled temperature and humidity conditions (25 °C, 50% RH) prior to sampling. After weight evaluation, the filter membrane is sealed and stored in a refrigerator for ion analysis.

2.2. Chemical Analysis. Water-soluble inorganic ions in $PM_{2.5}$ samples were quantitatively analyzed via ion chromatography (IC-8610, Qingdao Luhai Photoelectric Technology Company). The sample treatment process was as follows: filter membrane pieces (8.10 mm diameter) were cut out and placed in 10 mL of deionized water for 30 min. They were allowed to stand still for 60 min, followed by the supernatant being collected for analysis. Prior to the test, the linear repeatability of the ion chromatograph was tested, and several control samples were established for quality control. The chromatographic conditions were as follows: IonPac AS19 column was used in the anion mode; 25 mmol/L NaOH solution was used as eluent; flow rate was maintained at 1.2 mL/min; the detection limit (S/N = 3) was less than 0.02 mg/L; IonPac CS12 column was used in cation mode, where the eluent was a 30 mmol/L MSA solution; the flow rate was maintained at 1.00 mL/min; detection limit (S/N = 3) was less than 0.02 mg/L. In the analysis, several ions were evaluated, including Na^+, NH_4^+, K^+, Ca^{2+}, Mg^{2+}, F^-, Cl^-, NO_2^-, NO_3^-, and SO_4^{2-}.

https://doi.org/10.1021/acsomega.2c02919
ACS Omega 2022, 7, 35575−35585

The TOF-SIMS 5−100 (ION-TOF GmbH, Germany) instrument was used for SIMS analysis. A fixed 5 × 10 mm filter membrane sample was used in the SIMS sample holder during testing. The surface of the sample was sterilized by sputtering ion beam under ultra-high vacuum, and inorganic ions in the surface micro-area were analyzed under high-precision mass spectrometry mode. The spatial distribution characteristics of the surficial chemistry of the components of $PM_{2.5}$ samples were obtained by combining ion imaging mode with the response intensity. Mass spectrometry conditions were as follows: (1) primary ion beam: Bi_3^+ with an energy and ion current intensity of 30 KeV and 0.3 pA (pulse), respectively; (2) sputtering ion beam: Ar_n^+ with an energy and ion current intensity of 10 KeV and 6.4 nA, respectively, and sputtering time of 10 s; (3) neutralization electron gun: energy and electron current intensity are 21 eV and 15 μA, respectively. Further, vacuum degree, which represents the background of the main vacuum chamber, was less than 6 × 10^{-10} mbar; the time, which represents the analysis time of the imaging mode and high precision mass spectrometry mode, was 600 s; the analysis area was 50 × 50 μm; the secondary anions in the blank samples were mainly Si^+, SiO^+, and $SiOH^+$; and lastly, the cations were mainly O^-, OH^-, and SiO_2^-, among others.

2.3. Meteorological Data and Data Processing. Meteorological and air quality data for the Haidian District were collected during the sampling period (from December 18, 2017 to January 30, 2018 (see Annex 1 for details). Specifically, meteorological data were collected from the China Meteorological Data Network (http://data.cma.cn/), while air quality data were obtained from our monitoring site, that is, the Olympic Sports Center near the sampling site. The data were collected from the Beijing Environmental Protection Monitoring Center (http://www.bjmemc.com.cn/). The monitoring station is located northeast of the sampling site at a distance of 4.6 km (Figure 1).

2.4. Data Processing. The TOF-SIMS mass spectrometry data were processed using the data processing software, Surface Lab 6 (version 6.8), manufactured by the Ion-ToF Company, Germany. It was used to ensure quality correction and to perform imaging analysis. The corrected ion peaks belonged to H^+, C^+, and CH^{2+} in the cation mode, whereas in the anion mode, they pertain to H^-, O^-, and OH^-. Correlation and statistical analyses of the chromatographic data were performed via SPSS 19.0 software.

3. RESULTS AND DISCUSSIONS

3.1. Characteristics of Air Quality during the Sampling Period. The daily average concentrations of $PM_{2.5}$ and water-soluble inorganic ions during the sampling period are presented in Figure 2, and the point-line diagram depicts the simultaneous air quality index (AQI), which is often used to evaluate air quality comprehensively. According to the AQI classification standard,[31] the period in which AQI was ≤100 and air quality was evaluated to be excellent or of a good grade (hereinafter referred to as "clean period") lasted for 28 days. This accounts for 68.29% of the overall study period. The period during which AQI was >100 and air quality was evaluated to be slightly or moderately polluted (hereinafter referred to as "pollution period") spanned over 13 days, of which 9 days had slight pollution and 3 days had moderate pollution, while heavy pollution lasted only a day.

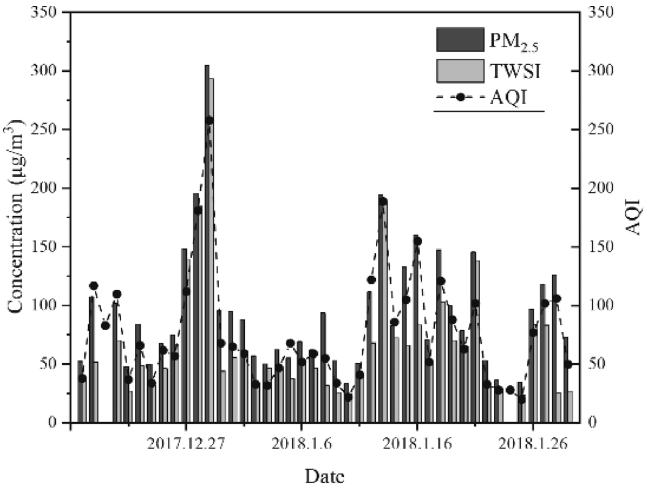

Figure 2. Daily variation of average mass concentration of $PM_{2.5}$ and water-soluble inorganic ions.

The main air pollutant during this period was evaluated as $PM_{2.5}$. Statistical results showed that the daily average mass concentration of $PM_{2.5}$ during the sampling period ranged from 33.57 to 305.01 $\mu g/m^3$, and the total average mass concentration was 94.28 ± 52.49 $\mu g/m^3$. According to the latest national standard, GB 3095-2012,[31] the permissible daily average mass concentration of $PM_{2.5}$ in urban residential areas is 75 $\mu g/m^3$. Referring to the standard limit, the number of days to meet the standard during the sampling period was 18 days, and the rate of reaching the standard was 43.9%. The average $PM_{2.5}$ concentrations in winter of Beijing for the three study years (2015−2017) were 106, 103, and 74 $\mu g/m^3$,[32−34] respectively. As compared to the winter of 2016, the average $PM_{2.5}$ concentration in the winter of 2017 decreased by 29 $\mu g/m^3$ (28.2% decrease). The data indicate that the air quality of Beijing in winter has been significantly improved in recent years, especially following the implementation of "coal-to-gas" policy during summer seasons in Beijing, Tianjin, and Hebei in 2017. The decline of $PM_{2.5}$ is closely associated with decreasing coal consumption, increasing usage of natural gas, requiring coal-fired power plants to install flue-gas desulfurization−denitrogenating systems, and the implementation of a stricter vehicular emission standard. In addition, it may be also due to the abnormal winter climate in Beijing and surrounding areas in that year. Illustratively, the East Asian winter monsoon circulation system in 2017 was strong, and the abnormally cold low-pressure system was conducive for the vertical diffusion of pollutants.

3.2. Concentration of Water-Soluble Inorganic Ions in $PM_{2.5}$. The results of ion chromatography analysis showed that the total concentration of inorganic ranged from 23.47 to 293.50 $\mu g/m^3$, with an average concentration of 67.12 ± 53.07 $\mu g/m^3$. The variation trend of daily average concentration of water-soluble inorganic ions is similar to that of $PM_{2.5}$ during the sampling period. Overall, the total water-soluble inorganic ions (TWSII) accounted for a large proportion of $PM_{2.5}$ concentration, ranging from 20.2 to 97.5%, with an average of 68.2%. For TWSII, the average proportions of the main anions and cations are as follows: NO_3^- (31.5%), SO_4^{2-} (23.4%), Cl^- (6.6%), Ca^{2+} (16.3%), NH_4^+ (6.6%), K^+ (4.6%); they reached 89%.

Under different air quality conditions, the concentration and proportion of water-soluble inorganic ions varied markedly

https://doi.org/10.1021/acsomega.2c02919
ACS Omega 2022, 7, 35575−35585

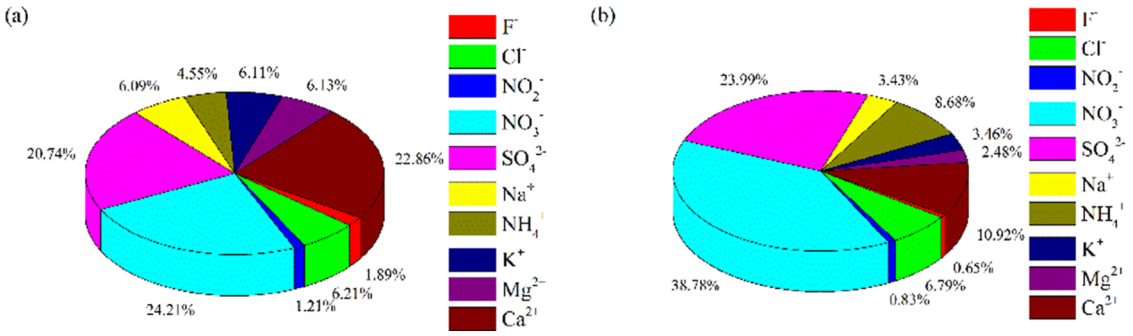

Figure 3. Water-soluble inorganic ion composition of $PM_{2.5}$ during sampling day: (a) clean period; (b) pollution period.

Table 1. Concentration of $PM_{2.5}$ and Water-Soluble Inorganic Ions during the Pollution Period

NO	F^-	Cl^-	NO_2^-	NO_3^-	SO_4^{2-}	Na^+	NH_4^+	K^+	Mg^{2+}	Ca^{2+}	WSII	$PM_{2.5}$
1	0.60	4.50	2.00	17.31	10.71	1.63	1.41	2.36	2.75	8.35	51.62	107.42
2	0.61	6.43	4.68	28.77	8.75	2.31	4.52	1.84	2.22	10.16	70.29	102.08
3	1.08	8.90	0.48	56.92	42.88	2.68	14.26	2.47	2.03	7.83	139.53	148.26
4	0.53	7.97	0.72	86.12	42.87	2.81	22.24	2.23	2.58	16.69	184.76	195.62
5	0.71	7.83	0.61	27.79	9.57	1.69	4.14	2.79	2.29	10.71	68.13	305.01
6	0.60	20.43	0.43	87.27	42.06	2.47	20.63	2.67	2.85	10.37	189.78	111.66
7	0.69	3.45	0.40	15.19	14.27	4.80	2.02	3.04	2.65	19.71	66.22	194.59
8	0.60	4.93	0.51	25.88	15.98	8.39	2.48	11.70	2.27	10.71	83.45	132.85
9	0.68	8.64	0.50	48.93	18.43	2.35	5.57	3.60	3.04	11.30	103.04	160.36
10	1.87	6.84	1.22	22.51	35.99	15.93	8.40	11.02	6.58	28.18	138.54	147.58
11	0.60	6.66	0.36	36.84	18.35	1.22	4.03	3.32	2.22	9.66	83.26	145.72
12	0.60	1.32	0.00	2.61	6.00	0.88	0.30	2.35	2.37	9.04	25.47	117.86
13	0.58	13.76	0.47	124.56	93.37	4.17	39.97	2.38	3.36	10.88	293.50	126.18
min	0.53	1.32	0.00	2.61	6.00	0.88	0.30	1.84	2.03	7.83		
max	1.87	20.43	4.68	124.56	93.37	15.93	39.97	11.70	6.58	28.18		
mean	0.75	7.82	0.95	44.67	27.63	3.95	10.00	3.98	2.86	12.58	115.20	153.48
SD	0.36	4.84	1.22	33.87	23.18	4.10	11.06	3.31	1.18	5.74		

(Figure 3a,b). The total daily average mass concentration of water-soluble inorganic ions was 44.80 ± 16.08 $\mu g/m^3$ in the clean period, accounting for 67.07% of the total mass concentration of $PM_{2.5}$. The proportion of each component is shown in Figure 3a; NO_3^-, Ca^{2+}, and SO_4^{2-} accounted for the largest proportions (24.21, 22.86, and 20.74%), respectively. From the ionic ratio, it can be inferred that alkali metal (K^+ and Na^+) and alkaline earth metal (Ca^+ and Mg^+) ions were the main components of cations, while NH_4^+accounted for only 4.55% of the ions. Furthermore, the main anions were NO_3^-, SO_4^{2-}, and Cl^-. As compared to previous research results, the concentration of Ca^+ and Mg^+ from the crustal source was higher in this study, of which Ca^{2+} accounted for 22.86% during the good period, with an average concentration of 12.58 ± 5.51 $\mu g/m^3$, which is much higher than that during the same period in recent years.[35,36] The increase in Ca^+ and Mg^+ concentrations may be due to the abnormal winter climate in Beijing and surrounding areas in that year. Illustratively, the East Asian winter monsoon circulation system in 2017 was strong, and the lower atmosphere turned into an abnormally cold low-pressure system, which was conducive for the vertical diffusion of pollutants.[37] Aside from the decrease in the overall $PM_{2.5}$ concentration in Beijing, the frequent influx of cold air in North China also generated more dust, resulting in a sharp increase in the concentration of crustal ions.

The total daily average mass concentration of water-soluble inorganic ions in the pollution period was 115.20 ± 70.29 $\mu g/m^3$, accounting for 75.06% of the total concentration of $PM_{2.5}$. As shown in Figure 3b, NO_3^-, SO_4^{2-}, Ca^{2+}, and NH_4^+ accounted for the largest proportions as follows: 38.78, 23.99, 10.92, and 8.68%, respectively. Compared to the clean period, the concentration of SNA ions considerably increased. The average concentrations of NO_3^-, SO_4^{2-}, and NH_4^+ increased from 10.85 ± 8.11, 9.29 ± 4.30, and 2.04 ± 1.92 $\mu g/m^3$ to 44.67 ± 33.87, 27.63 ± 23.18, and 10.00 ± 11.06 $\mu g/m^3$, respectively. The total average values of NO_3^-, SO_4^{2-}, and NH_4^+ were 21.57 ± 25.62, 15.11 ± 16.00, and 4.56 ± 7.42 $\mu g/m^3$, respectively (Tables 1 and 2). Compared with 2016, the concentration of SO_4^{2-} and NH_4^+ decreased.[38] Moreover the three ions increased by 312, 197, and 390%, respectively. The total concentration of the three ions in $PM_{2.5}$ increased from 49.51 to 71.44%, corresponding to clean and pollution periods, respectively. Concentrations and proportions of Cl^-, NO_2^-, and F^- ions did not fluctuate significantly during either period; however, the proportion of K^+, Na^+, Ca^+, and Mg^+ ions decreased considerably, especially Ca^+, during the pollution period (Figure 3) (from 22.86 to 10.92%, corresponding to the respective clean and pollution periods).

From the abovementioned data, it can be inferred that SNA is the main water-soluble inorganic ion component in $PM_{2.5}$. Furthermore, it constitutes the highest proportion of water-soluble inorganic ions during the pollution period. The data also revealed that the increase in SNA mass concentration was the main factor that led to an increase in $PM_{2.5}$ mass concentration during the pollution period. Interestingly, Jia et

https://doi.org/10.1021/acsomega.2c02919
ACS Omega 2022, 7, 35575−35585

Table 2. Concentration of $PM_{2.5}$ and Water-Soluble Inorganic Ions during the Clean Period

NO	F^-	Cl^-	NO_2^-	NO_3^-	SO_4^{2-}	Na^+	NH_4^+	K^+	Mg^{2+}	Ca^{2+}	TWSII	$PM_{2.5}$
1	0.68	1.44	0.82	3.85	13.7	2.12	0.31	4.09	2.37	8.9	38.29	52.34
2	1.5	1.58	0.46	5.12	5.77	0.77	0.2	1.59	2.07	7.83	26.88	47.91
3	0.64	3.32	1.1	14.88	10.84	2.2	0.55	2.24	2.45	10.36	48.58	84.11
4	0.87	1.53	0.45	4.2	5.9	3.04	0.69	2.46	2.48	10.06	31.66	49.72
5	0.63	2.53	0.52	15.53	9.96	1.34	2.64	2.32	2.25	8.63	46.34	67.63
6	0.9	8.09	0.47	20.59	12.67	3.74	4.93	3.43	2.35	9.15	66.31	75.03
7	0.63	3.94	0.35	9.37	9.76	2.43	0.54	2.97	2.86	11.44	44.29	95.51
8	0.7	3.74	0.67	16.75	11.47	2.04	5.91	1.89	2.37	10.1	55.65	95.16
9	0.7	6.27	0.36	16.88	11.7	2.96	6.2	3.87	2.75	9.64	61.33	87.86
10	0.54	1.11	0.38	6.33	7	1.86	0.7	2.05	2.4	10.78	33.14	57.07
11	0.54	1.27	0.53	4.49	7.16	2.48	0.34	2.85	2.73	24.2	46.59	50.21
12	0.96	2.49	1	7.82	7.81	3.53	5.64	3.47	2.49	11.17	46.38	62.42
13	1.39	1.1	0.36	9.94	6.03	2.06	1.56	2.82	2.54	9.74	37.55	55.32
14	1.75	4.98	0.53	11.53	5.88	7.68	2.41	2.33	2.35	10.74	50.17	69.29
15	1.05	0.92	0.52	11.26	11	1.69	2.12	2.9	2.68	12.55	46.67	62.24
16	0.74	1.02	0.45	2.43	7.47	2.04	0.5	2.47	2.51	12.42	32.06	93.75
17	0.83	0.9	0.61	2.5	5.3	1.06	1.19	1.73	2.19	9.54	25.85	53.22
18	1.09	1.22	0.45	2.22	3.4	0.74	1.44	1.89	2.09	9.93	24.48	33.57
19	0.58	1.8	0.42	8.57	5.95	5.79	2.49	2.18	2.24	8.35	38.37	50.59
20	0.88	2.67	0.45	28.44	19.27	1.24	4.83	2.86	2.5	9.22	72.35	82.93
21	0.56	4.22	0.36	9.66	18.09	2.57	1.38	2.18	2.21	10.18	51.39	70.9
22	0.53	5.45	0.37	28.41	14.9	1.8	4.32	2.67	2.26	9.57	70.28	99.9
23	1.32	4.92	0.77	11.45	12.39	6.94	3.63	4.49	3.78	15.77	65.47	78.74
24	0.63	1.1	0.37	5.03	6.83	2	1.2	1.86	2.21	9.25	30.49	53.3
25	1.1	1.11	0.39	5.9	5.24	1.08	0.43	2.6	2.26	9.15	29.27	36.46
26	0.54	1.3	0.35	4.66	2.84	3.09	0.15	3.04	4.22	3.27	23.47	34.81
27	0.8	6.64	1.16	32.08	16.32	7.09	0.37	4.83	9.03	5.65	83.98	96.98
28	0.61	1.21	0.5	3.8	5.4	1.08	0.43	2.6	2.26	9.15	27.05	73.16
min	0.53	0.9	0.35	2.22	2.84	0.74	0.15	1.59	2.07	3.27		
max	1.75	8.09	1.16	32.08	19.27	7.68	6.2	4.83	9.03	24.2		
mean	0.85	2.78	0.54	10.85	9.29	2.73	2.04	2.74	2.75	10.24	44.8	66.79
SD	0.32	2.01	0.22	8.11	4.3	1.87	1.92	0.81	1.29	3.43		

Table 3. Correlation Coefficients of $PM_{2.5}$ Water-Soluble Inorganic Ions in the Clean Period

correlation	F^-	Cl^-	NO_2^-	NO_3^-	SO_4^{2-}	Na^+	NH_4^+	K^+	Mg^{2+}	Ca^{2+}
F^-	1.000									
Cl^-	0.045	1.000								
NO_2^-	0.048	0.222	1.000							
NO_3^-	−0.063	0.731**	0.261	1.000						
SO_4^{2-}	−0.216	0.598**	0.269	0.752**	1.000					
Na^+	0.280	0.545**	0.362	0.291	0.146	1.000				
NH_4^+	0.059	0.539**	0.034	0.524**	0.407*	0.158	1.000			
K^+	0.020	0.503**	0.448*	0.407*	0.449*	0.524**	0.205	1.000		
Mg^{2+}	−0.038	0.375*	0.503**	0.463*	0.277	0.539**	−0.156	0.642**	1.000	
Ca^{2+}	0.021	−0.095	0.020	−0.204	0.006	0.028	0.019	0.040	−0.221	1.000

al.[36] analyzed the concentration of SNA in $PM_{2.5}$ samples collected in different seasons from 2014 to 2016 in Beijing and reported that the maximum concentrations of NO_3^-, SO_4^{2-}, and NH_4^+ions were prevalent in winter. The concentration of SNA increased significantly during the period of heavy air pollution, which is consistent with results of previous studies.

The mass concentration ratio of NO_3^- to SO_4^{2-} is often used to determine the contribution of fixed (coal-fired) and mobile (vehicle exhaust) sources to the mass concentration of particulate matter.[39] Whenever $[NO_3^-]/[SO_4^{2-}]$ is >1, it indicates that mobile sources contribute more to the mass concentration of $PM_{2.5}$ than do the fixed sources, whereas an inverse ratio results in an opposite/contrast outcome. As shown in Figure 3a,b, the proportions of NO_3^- during the clean and pollution periods were greater than those of SO_4^{2-}. Furthermore, the proportions of NO_3^- during the clean and pollution periods were evaluated as 1.12 and 1.77, respectively, and the average ratio of $[NO_3^-]/[SO_4^{2-}]$ was calculated as 1.43. These statistics show that NO_3^- and SO_4^{2-} in $PM_{2.5}$ mainly come from mobile sources representing exhaust pollution from vehicles. With the occurrence of pollution, the contribution of mobile sources to $PM_{2.5}$ becomes more significant. The main factors affecting the ratio of $[NO_3^-]/[SO_4^{2-}]$ during this period may include the following: (1) increase in the number of motor vehicles; enhancing the emission of gas pollutants from mobile sources (NO and NO_2, etc.), which results in the increase in NO_3^{2-} concentration; (2) the change in heating mode in Beijing and its surrounding

https://doi.org/10.1021/acsomega.2c02919
ACS Omega 2022, 7, 35575−35585

Table 4. Correlation Coefficients of $PM_{2.5}$ Water-Soluble Inorganic Ions in the Pollution Period[a]

correlation	F^-	Cl^-	NO_2^-	NO_3^-	SO_4^{2-}	Na^+	NH_4^+	K^+	Mg^{2+}	Ca^{2+}
F^-	1.000									
Cl^-	−0.057	1.000								
NO_2^-	0.010	−0.123	1.000							
NO_3^-	−0.202	0.798**	−0.187	1.000						
SO_4^{2-}	0.109	0.643*	−0.246	0.894**	1.000					
Na^+	0.804**	−0.065	−0.003	−0.122	0.178	1.000				
NH_4^+	−0.064	0.717**	−0.179	0.960**	0.965**	0.013	1.000			
K^+	0.561*	−0.175	−0.115	−0.270	−0.061	0.864**	−0.213	1.000		
Mg^{2+}	0.829**	0.091	0.003	0.004	0.280	0.842**	0.145	0.559*	1.000	
Ca^{2+}	0.703**	−0.122	−0.033	−0.118	0.102	0.807**	0.007	0.512	0.814**	1.000

[a]Note: * Significant correlation at 0.05 level (bilateral) and ** Significant correlation at 0.01 level (bilateral).

areas in the winter reduces sulfur emission from fixed sources, which is one of the benefits of the "coal-to-gas" policy and the implementation of coal-firing control measures, such as clean energy transformation of traditional coal-fired boilers.

3.3. Existing Forms of Water-Soluble Inorganic Ions in $PM_{2.5}$. *3.3.1. Correlation Analysis of Mass Concentration.* Correlation analysis was performed on 10 water-soluble inorganic ions observed in samples collected during the clean and pollution periods, using the SPSS 20.0 software. The results are presented in Tables 3 and 4. Generally, a good correlation between ions is observed when they maintain a chemical quantitative relationship during atmospheric transport, enhancing the analysis of their possible sources and molecular binding forms. Our results showed that there was a good correlation between Cl^- and NO_3^-, as well as Cl^- and SO_4^{2-}, during the good period, with correlation coefficients of 0.731 and 0.598, respectively. Similarly, K^+ and Mg^{2+} had a significantly higher correlation coefficient of 0.642, while the correlation between other ions was not significant. Notably, there were no anion−cation combinations with high correlation coefficients.

As compared to the clean period, water-soluble inorganic ions during the polluted period exhibited better correlation. The correlation coefficients between NO_3^- and SO_4^{2-} and those between NO_3^- and NH_4^+ were approximately 0.9, which indicated that SNA ions came from the same pollution source and were closely related in their molecular morphologies. Furthermore, good correlations were observed between (F^- and Na^+) and (Mg^{2+} and Ca^{2+}), and the correlation coefficients were above 0.7. Correlation coefficients greater than 0.63 were observed between (Cl^- and NO_3^-) and (Cl^- and SO_4^{2-}), indicating that the SNA ions had a similar pollution source and were closely related in their molecular morphologies.

Table 4 shows that there was a good correlation between NH_4^+ ion and anions, such as SO_4^{2-}, NO_3^-, and Cl^-, whose correlation coefficients were as high as 0.965, 0.960, and 0.717, respectively. However, when the mass concentrations of the pairs of NH_4^+ with SO_4^{2-}, NO_3^-, and Cl^- were converted to their equivalent concentrations, there was no good correlation between their mass concentrations during the clean period (Figure 4a,c,e). Contrastingly, the equivalent concentrations of SNA during the polluted period were significantly correlated. As shown in Figure 4b,d, R^2 is above 0.9, and the relative slopes of the regression equations are1.23 and 1.07, respectively. This indicated that the ratio of equivalent concentration was approximately 1:1. Furthermore, NH_4^+ and Cl^- ions exhibited a good correlation (R^2 = 0.470); however, the slope is 3.35. As shown in Figure 7f, the main molecular form of NH_4^+ existed as $(NH_4)_2SO_4$ or NH_4NO_3 instead of NH_4Cl. Notably, it was difficult to evaluate these major forms of existence depending only on correlation analysis.

3.3.2. TOF-SIMS Analysis. Results obtained from TOF-SIMS imaging of typical samples (sample number 10, Figure 4b, point B) collected during the pollution period are shown in Figure 5. The results indicated that the surface of $PM_{2.5}$ samples collected during this period mainly composed of cations and anions, such as NH_4^+, NO_3^-, NO_2^-, SO_3^-, SO_4^-, HSO_4^-, F^-, Cl^-, K^+, Na^+, Ca^+, and Mg^+. Among these, NO_3^- and NO_2^- are fragments of nitrate (NO_x^-) created during the mass spectrometric analysis, while SO_3^-, SO_4^- and $HSO_4^-$are characteristic ion peaks originating from sulfate (SO_x^-).[21,41] The brightness of the image reflects the mass spectrum response intensity of each ion. As shown in Figure 5, cations and anions with higher surface response intensities are as follows: (K^+, Na^+, NH_4^+) and (HSO_4^-, SO_4^-, SO_3^-, NO_3^-,Cl^-), respectively. All other ions had relatively low response intensity. This reveals that SNA ions constitute a large proportion of the surface of particulate matter. Salts of NH_4^+, SO_4^{2-}, NO_3^-, K^+, and Na^+ ions were revealed as the main inorganic components on the surface of $PM_{2.5}$ during the pollution period.

The clean period is represented by sample number 12 (Figure 4a, point A), and the analysis results are shown in Figure 6. As compared to the pollution period, the response intensity of ions on the surface of $PM_{2.5}$ samples varied greatly during the clean period. As shown in Figure 6a−f, the intensity of NH_4^+, NO_3^-, NO_2^-, SO_3^-, SO_4^-, and HSO_4^- ions decreased by varying degrees, of which Ca^{2+}, SO_3^-, SO_4^-, HSO_4^-, and NH_4^+ ions are remarkable. Furthermore, Cl^-, K^+, and Na^+ were identified as the particles in the field of vision with no obvious variation in the strength of other ions.

As compared to the TOF-SIMS analysis results for the two groups of samples, it was easily identified that the strength of SNA ions on the $PM_{2.5}$ surface during the pollution period is much higher than that in the good period, which indicated that there were significant differences in the concentration of SNA ions on the $PM_{2.5}$ surface under different air quality conditions. Sulfate, nitrate, and ammonium salts formed by SNA ions have an important influence on the hygroscopic growth characteristics of atmospheric aerosols.[40] As shown in Figure 5a−l, during the pollution period with high relative humidity (RH = 77.17%), the SNA-rich aerosol particles react with water, as well as SO_x and NO_y, in the atmosphere during the long-term sampling process, forming secondary aerosols with increased mass and volume following deliquescence and weathering.[4]

https://doi.org/10.1021/acsomega.2c02919
ACS Omega 2022, 7, 35575−35585

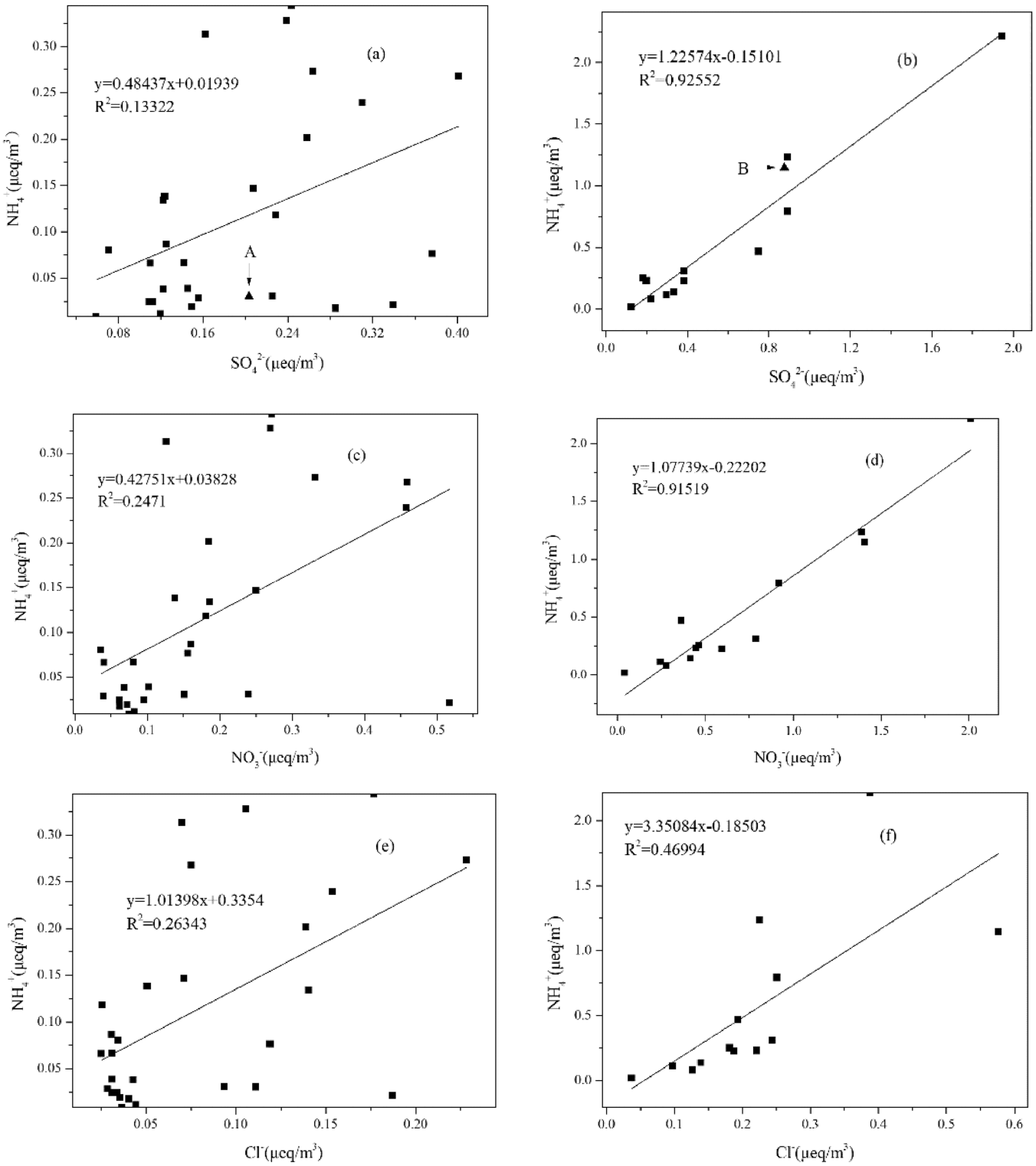

Figure 4. Equivalent concentration correlation of NH_4^+ and SO_4^{2-}, NO_3^-, and Cl^-; left side (a,c,e): clean period; right side (b,d,f): pollution period.

Therefore, the average particle size of $PM_{2.5}$ during the pollution period was slightly larger than that of the clean period (Figure 6a–l), which further showed that there were lots of SO_4^{2-}, NO_3^{2-}, and NH_4^+ salts on the surface of $PM_{2.5}$ during the pollution period.

By comparing the spatial distribution characteristics of each ion image, we can further discuss the main molecular forms of SNA ions on the $PM_{2.5}$ surface in different periods. For the pollution period, the surface of $PM_{2.5}$ mainly constituted the SNA ions, of which the NH_4^+ (Figure 5a) ion image was highly coincidental with those of SO_3^-, SO_4^-, and HSO_4^- (Figure 5d–f), which were quite different from those of NO_2^- and NO_3^- (Figure 5b,c), indicating that the main types of $PM_{2.5}$ were probably $(NH_4)_2SO_4$ and NH_4HSO_4, while the proportion of NH_4NO_3 and NH_4Cl was relatively small. During the clean period, the content of SNA ions (Figure 6a–

https://doi.org/10.1021/acsomega.2c02919
ACS Omega 2022, 7, 35575−35585

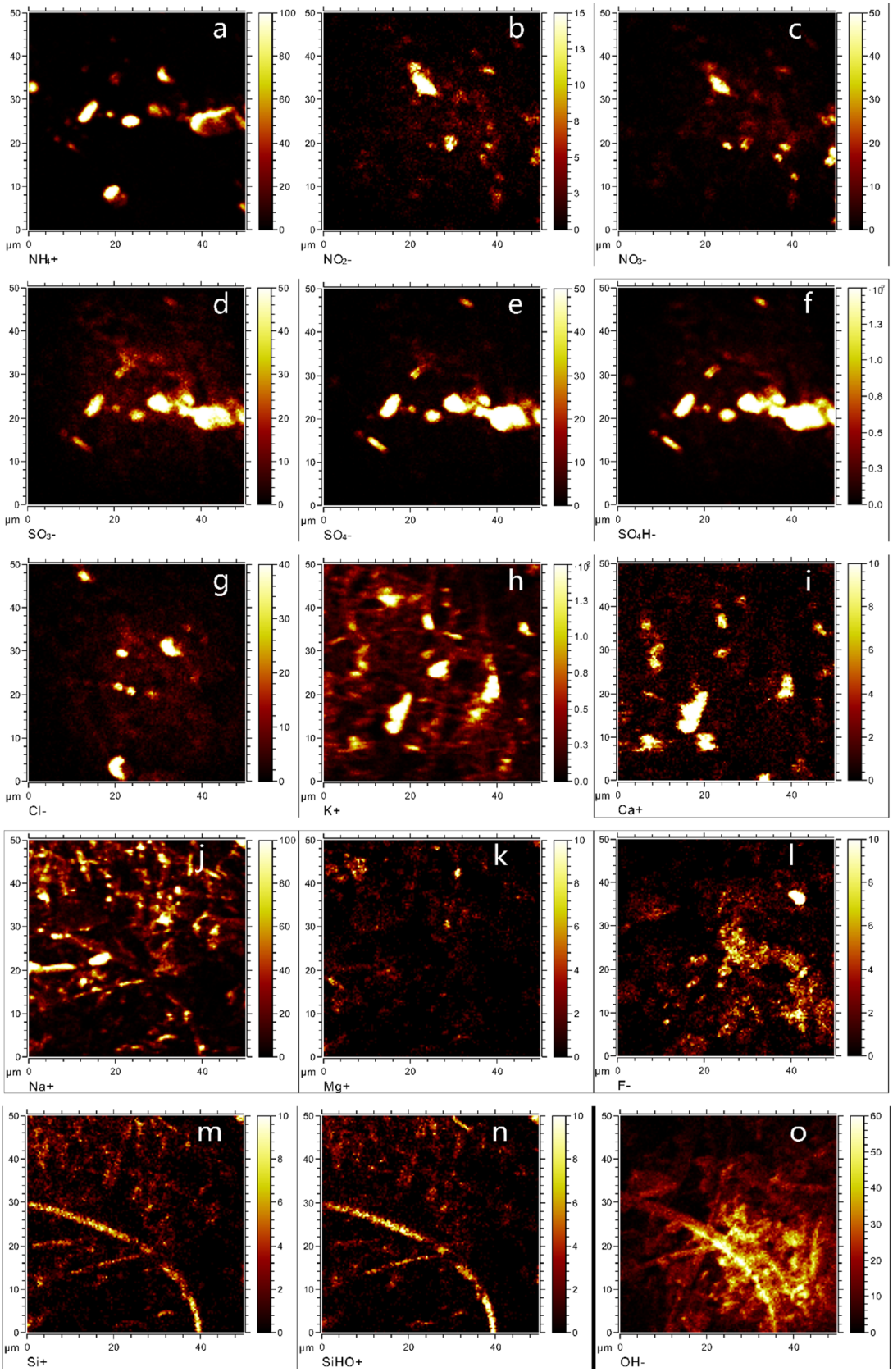

Figure 5. TOF-SIMS imaging results of $PM_{2.5}$ samples during the pollution period (AQI: 180.79; a, NH_4^+; b, NO_2^-; c, NO_3^-; d, SO_3^-; e, SO_4^-; f, SO_4H^-; g, Cl^-; h, K^+; i, Ca^+; j, Na^+; j, K^+; l, F^-; m, Si^+; n, $SiHO^+$; o, OH^-).

f) was low, and the correlation was poor. Furthermore, NH_4^+ ions exist in $PM_{2.5}$ with strong characteristics, implying that NH_4^+ is more likely to form $(NH_4)_2SO_4$ and NH_4HSO_4 molecules than NH_4NO_3 and NH_4Cl. This phenomenon was

https://doi.org/10.1021/acsomega.2c02919
ACS Omega 2022, 7, 35575−35585

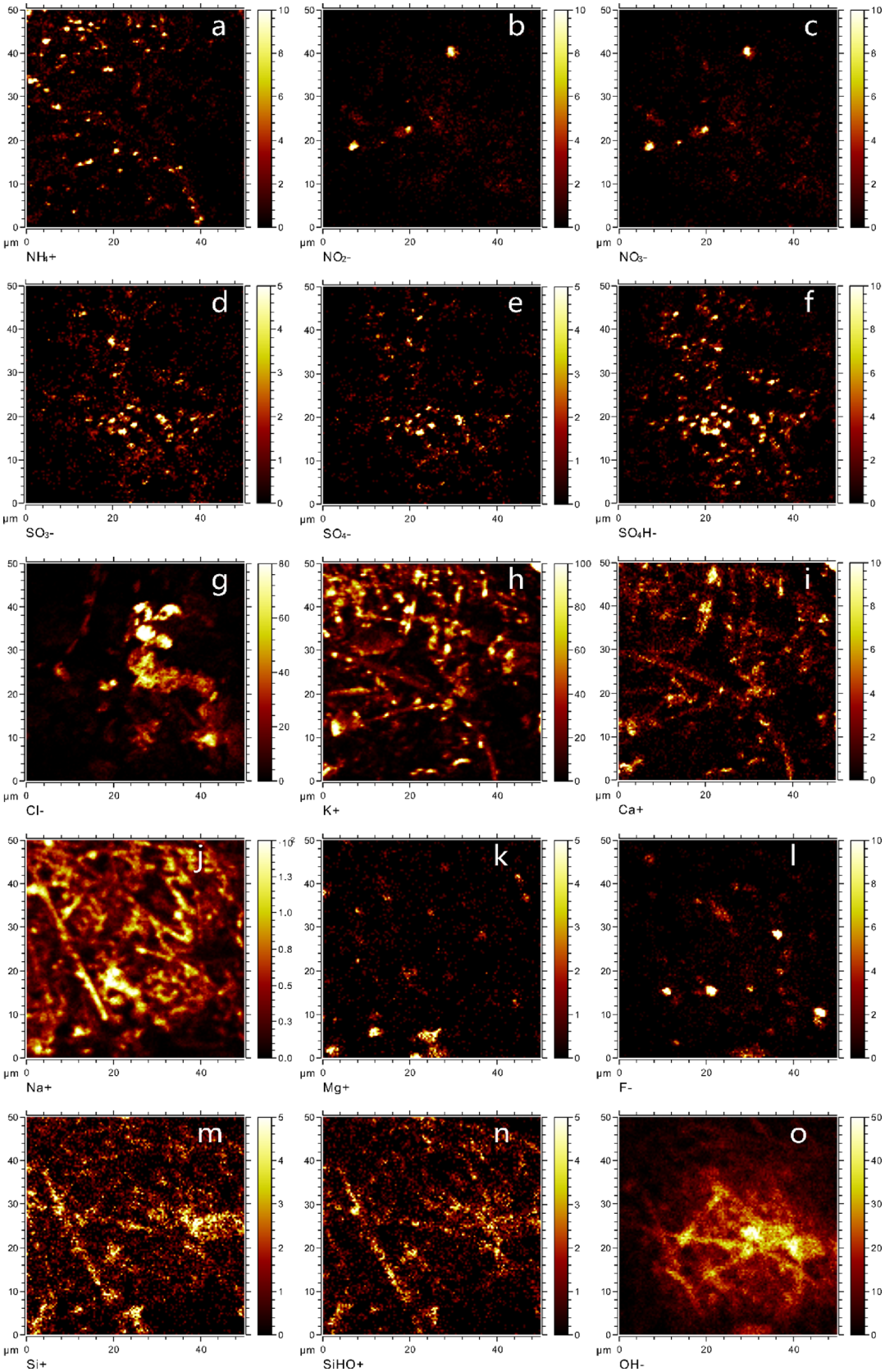

Figure 6. TOF-SIMS imaging results of $PM_{2.5}$ samples the good period (AQI: 67.92; a, NH_4^+; b, NO_2^-; c, NO_3^-; d, SO_3^-; e, SO_4^-; f, SO_4H^-; g, Cl^-; h, K^+; i, Ca^+; j, Na^+; j, K^+; l, F^-; m, Si^+; n, $SiHO^+$; o, OH^-).

also reported in the study of $PM_{2.5}$ in Beijing winters in 2015.[23] The reason for the selective binding of NH_4^+ in $PM_{2.5}$ may be attributed to the chemical properties of NH_4^+ salts. Zhang et al.[41] proposed that NH_4^+ ions can exist in many forms in

https://doi.org/10.1021/acsomega.2c02919
ACS Omega 2022, 7, 35575−35585

$PM_{2.5}$; however, $(NH_4)_2SO_4$ is the most stable form, followed by NH_4NO_3, while NH_4Cl is most unstable and volatile. Thus, NH_4^+ in $PM_{2.5}$ will bind to SO_4^{2-}, NO_3^-, and Cl^- in a successive or respective manner.

4. CONCLUSIONS

(1) In the winter of 2017, the average mass concentration of $PM_{2.5}$ in Beijing was recorded to be 94.28 ± 52.49 $\mu g/m^3$, which was 28.2% lower than that in the previous year. During the sampling period, the number of clean days was 28, which accounted for 68.29% of the overall days considered. The number of polluted days was only 13 without serious pollution, and the air quality was considerably improved.

(2) The ions, NO_3^-, Ca^{2+}, SO_4^{2-}, and Cl^-, were predominant during the clean period. In contrast, the predominant ions during the days of pollution were mainly NO_3^-, SO_4^{2-}, Ca^{2+}, and NH_4^+. In contrast, the predominant ions during the days of pollution were mainly NO_3^-, SO_4^{2-}, Ca^{2+}, and NH_4^+. Furthermore, the proportion of SNA increased significantly in the clean period, and the increase in the water-soluble ion mass concentration was the main factor that caused an increase in $PM_{2.5}$ mass concentration during the pollution period. Correlation analysis of 10 various water-soluble ions in the clean and pollution periods revealed that the correlation of NH_4^+ with SO_4^{2-} and NO_3 was equivalent, while the concentration of the latter ion was significantly higher than that of the former. This indicated that there might be $(NH_4)_2SO_4$ or NH_4NO_3 molecules during the pollution period.

(3) The results of TOF-SIMS analysis showed that there were significant differences in water-soluble inorganic ions on the $PM_{2.5}$ surface under different air quality conditions. Compared to the clean period, the response intensity of SNA ions on the $PM_{2.5}$ surface was higher during the pollution period, while other components did not change much, indicating that SNA was the main ion type on the $PM_{2.5}$ surface during the pollution period. Ion imaging analysis further explored the molecular composition of SNA ions. As per the correlation analysis between NH_4^+ and SO_4^{2-} ions, ammonium sulfate or ammonium bisulfate was the main forms of NH_4^+ salts on the $PM_{2.5}$ surface during the pollution period.

AUTHOR INFORMATION

Corresponding Authors

Kang Yang − *School of Chemical & Environmental Engineering, CUMTB, Beijing 100083, China;* orcid.org/0000-0002-0776-0921; Email: ykjrtuy@sina.com

Handong Liang − *State Key Laboratory of Coal Resources and Safe Mining, CUMTB, Beijing 100083, China;* Email: 475427038@qq.com

Authors

Xiuping Hong − *Huaibei Normal University, Huaibei 235000, China*

Yunyun Shi − *School of Chemical & Environmental Engineering, CUMTB, Beijing 100083, China*

Complete contact information is available at: https://pubs.acs.org/10.1021/acsomega.2c02919

Notes

The authors declare no competing financial interest.

ACKNOWLEDGMENTS

This work was supported by Anhui Natural Science Foundation Project (No. 2008085QD169), the National Natural Science Foundation of China (Nos. 41902172 and 41772157), and the Natural Science Research Project of Colleges and Universities in Anhui Province (No. KJ2020A1204).We would like to give special thanks to Ou Yang, Qin Zhan, and Jiang Wu for their support with the sampling.

REFERENCES

(1) Wang, Y.; Zhang, Q. Q.; He, K.; Zhang, Q.; Chai, L. Sulfate-nitrate-ammonium aerosols over China: response to 2000-2015 emission changes of sulfur dioxide, nitrogen oxides and ammonia. *Atmos. Chem. Phys. Discuss.* **2013**, *13*, 2635−2652.

(2) Zhang, Z. Y.; Zhang, X. L.; Gong, D. Y.; Quan, W. J.; Ma, Z. Q.; Kim, S. J. Evolution of surface O_3 and $PM_{2.5}$, concentrations and their relationships with meteorological conditions over the last decade in Beijing. *Atmos. Environ.* **2015**, *108*, 67−75.

(3) Yu, Y. Y.; Ding, F.; Mu, Y. F.; Xie, M. J.; Wang, Q. G. High time-resolved $PM_{2.5}$ composition and sources at an urban site in Yangtze River Delta, China after the implementation of the APPCAP. *Chemosphere* **2020**, *261*, No. 127746.

(4) Zhang, Y. Y.; Tang, A. H.; Wang, C.; Ma, X.; Li, Y. Z.; Xu, W.; Xia, X. P.; Zheng, A. H.; Li, W. Q.; Fang, Z. G.; Zhao, X. F.; Peng, X. L.; Zhang, Y. P.; Han, J.; Zhang, L. J.; Collett, J. L., Jr.; Liu, X. J. $PM_{2.5}$ and water-soluble inorganic ions concentrations decreased faster in urban than rural areas in China. *J. Environ. Sci.* **2022**, *122*, 83−91.

(5) Zhao, X. X.; Zhao, X. J.; Liu, P. F.; Ye, C.; Xue, C. Y.; Zhang, C. L.; Zhang, Y. Y.; Liu, C. T.; Liu, J. F.; Chen, H.; Chen, J. M.; Mu, Y. J. Pollution levels, composition characteristics and sources of atmospheric $PM_{2.5}$ in a rural area of the North China Plain during winter. *J. Environ. Sci.* **2020**, *95*, 172−182.

(6) Ding, M. M.; Zhou, J. N.; Liu, B. X.; Wang, Y.; Zhang, B. T.; Shi, A. J. Characteristics of NO_3^-, SO_4^{2-}, NH_4^+ of $PM_{2.5}$ and their precursor gas during 2015 in a urban area of Beijing. *Environ. Sci.* **2017**, *38*, 1307−1316.

(7) Geng, G.; Xiao, Q.; Zheng, Y.; Tong, D.; Zhang, Y.; Zhang, X.; Zhang, Q.; He, K.; Liu, Y. Impact of China's Air Pollution Prevention and Control Action Plan on $PM_{2.5}$ chemical composition over eastern China. *Sci. China: Earth Sci.* **2019**, *62*, 1872−1884.

(8) Xiang, P.; Zhou, X. M.; Duan, J. C.; Tan, J. H.; He, K. B.; Cheng, Y.; Ma, Y. L. Chemical characteristics of water-soluble organic compounds (WSOC) in $PM_{2.5}$ in Beijing, China: 2011−2012. *Atmos. Res.* **2016**, *183*, 104−112.

(9) Zhang, Y. Y.; Lang, J. L.; Cheng, S. Y.; Li, S. Y.; Chen, D. S.; Zhang, H. Y. Chemical composition and sources of PM1 and PM2.5 in Beijing in autumn. *Sci. Total Environ.* **2018**, *630*, 72−82.

(10) Li, H. Y.; Cheng, J.; Zhang, Q.; Zheng, B.; Zhang, Y. X.; Zheng, G. J.; He, K. B. Rapid transition in winter aerosol composition in Beijing from 2014 to 2017: response to clean air actions. *Atmos. Chem. Phys.* **2019**, *19*, 11485−11499.

(11) Zhang, Z. W.; Hu, G. R.; Yu, R. L.; Hu, Q. C.; Liu, X. R. Characteristics and sources apportionment of water-soluble ions in $PM_{2.5}$ Xiamen city, China. *China Environ. Sci.* **2016**, *36*, 1947−1954.

(12) Yao, Q.; Liu, Z. R.; Han, S. Q.; Cai, Z. Y.; Liu, J. L.; Huang, X. J. *Environ. Sci.* **2017**, *38*, 1−13.

(13) Liu, K. K.; Ren, J. Seasonal characteristics of $PM_{2.5}$ and its chemical species in the northern rural China. *Atmos. Pollut. Res.* **2020**, *11*, 1891−1901.

(14) He, K.B. *Atmospheric particulate matter and regional compound pollution*; Science Press: Beijing, 2011; pp 234−236.

(15) Xie, Y. J.; Lu, H. B.; Yi, A. J.; Zhang, Z. Y.; Zheng, N. J.; Fang, X. Z.; Xiao, H. Y. Characterization and source analysis of water−

soluble ions in PM2.5 at a background site in Central China. *Atmos. Res.* **2020**, *239*, No. 104881.
(16) Li, L. J.; Wang, Z. S.; Zhang, D. W.; Chen, T.; Jiang, L.; Li, Y. T. Analysis of heavy air pollution episodes in Beijing during 2013−2014. *China Environ. Sci.* **2016**, *36*, 27−35.
(17) Wu, D.; Lin, S. L.; Yang, H. Q.; Du, R. G.; Xia, J. R.; Qi, B. Pollution characteristics and light extinction contribution of water-soluble ions of $PM_{2.5}$ in Hangzhou. *Environ. Sci.* **2017**, *38*, 2656−2666.
(18) Huang, R. J.; Zhang, Y.; Bozzetti, C.; Ho, K. F.; Cao, J. J.; Han, Y. M.; Daellenbach, K. R.; Slowik, J. G.; Platt, S. M.; Canonaco, F.; Zotter, P.; Wolf, R.; Pieber, S. M.; Bruns, E. A.; Crippa, M.; Ciarelli, G.; Piazzalunga, A.; Schwikowski, M.; Abbaszade, G.; Schnelle-Kreis, J.; Zimmermann, R.; An, Z.; Szidat, S.; Baltensperger, U.; Haddad, I. E.; Prévôt, A. S. H. High secondary aerosol contribution to particulate pollution during haze events in China. *Nature* **2014**, *514*, 218.
(19) Murari, V.; Kumar, M.; Singh, N.; Singh, R. S.; Banerjee, T. Particulate morphology and elemental characteristics: variability at middle indo-Gangetic Plan. *J. Atmos. Chem.* **2016**, *73*, 165−179.
(20) Shi, J.; Zhang, G.; An, H.; Yin, W. L.; Xia, X. L. Quantifying the particulate matter accumulation on leaf surface of urban plants in Beijing, China. *Atmos. Pollut. Res.* **2017**, *8*, 836−842.
(21) Fletcher, J. S.; Vickerman, J. C. TOF-SIMS analysis of atmospherically relevant sulphuric acid hydrate films and reactions thereof. *Appl. Surf. Sci.* **2004**, *231*−*232*, 524−527.
(22) Li, W. J.; Sun, L. H.; You, W.; Tian, S. S.; Wang, L. X.; Zhao, Y. B.; Li, Z. P. Gender Recognition of Fingerprint Remnant Based on Time-of-Flight Secondary Ion Mass Spectrometry Imaging Signal of Fingerprint Substance. *Chin. J. Anal. Chem.* **2022**, *50*, 112−118.
(23) Yang, O.; Liang, H. D.; Li, Z. P.; Liu, Y. H. TOF-Sims characterization of ammonium single particles within $PM_{2.5}$. *J. Chin. Mass Spectrom. Soc.* **2018**, *39*, 722−728.
(24) Fang, C. L.; Wang, Z. B.; Xu, G. Spatial-temporal characteristics of $PM_{2.5}$ in China: A city-level perspective analysis. *J. Geogr. Sci.* **2016**, *26*, 1519−1532.
(25) Zhang, X.; Xu, X.; Ding, Y.; Liu, Y.; Zhang, H.; Wang, Y.; Zhong, J. The impact of meteorological changes from 2013 to 2017 on $PM_{2.5}$ mass reduction in key regions in China. *Sci. China: Earth .Sci.* **2019**, *62*, 1885−1902.
(26) The average concentration of $PM_{2.5}$ in Beijing from January to July was 14.1% lower than that in January to July. *Environ. Econ.* **2018**, *16*, 7.
(27) Zhang, Q.; Zheng, Y.; Tong, D.; Shao, M.; Wang, S.; Zhang, Y. Drivers of improved PM2.5 air quality in China from 2013 to 2017. *Proc. Natl. Acad. Sci. U. S. A.* **2019**, *116*, 24463−24469.
(28) Gao, L. M. Coal-to-Gas Process in China and Current Status Analysis. *Gas Heat* **2020**, *40*, 20−22.
(29) Wen, Z.; Wang, C. J.; Li, Q.; Xu, W.; Lu, L.; Li, X. J.; Tang, A. H.; Collett, J. L., Jr.; Liu, X. J. Winter air quality improvement in Beijing by clean air actions from 2014 to 2018. *Atmos. Res.* **2021**, *259*, No. 105674.
(30) Cheng, J.; Su, J.; Cui, T.; Li, X.; Dong, X.; Sun, F.; Yang, Y.; Tong, D.; Zheng, Y.; Li, Y.; Li, J.; Zhang, Q.; He, K. Dominant role of emission reduction in $PM_{2.5}$ air quality improvement in Beijing during 2013−2017: a model-based decomposition analysis. *Atmos. Chem. Phys.* **2019**, *19*, 6125−6146.
(31) Ministry of Environmental Protection. *GB 3095−2012 Ambient air quality standard*; China Environmental Science Press: Beijing, 2012.
(32) Cui, J. X.; Lang, J. L.; Chen, T.; Zhang, D. W.; Wang, Z. S.; Cheng, S. Y. Characteristics of Beijing's Air Quality and Regional Transport of $PM_{2.5}$ in 2016. *J. Beijing Univ. Technol.* **2018**, *44*, 1547−1556.
(33) Lou, J. Characteristics of the spatial and temporal distribution $PM_{2.5}$ in Beijing in 2017. *Sci. Technol. Innovation Herald* **2018**, *44*, 1547−1556.
(34) Yang, D. Y.; Liu, B. X.; Zhang, D. W.; Chen, Y. Y.; Zhou, J. N.; Liang, Y. P. Correlation, seasonal and temporal variation of water-soluble ions of $PM_{2.5}$ in Beijing during 2012−2013. *Environ. Sci.* **2015**, *36*, 768−773.
(35) Cong, X. G.; Cheng, L. L.; Wang, L. L.; Wang, G. A.; Liu, Y. S.; Li, X. R. The mass concentrantion levels, diurnal variation and source apportionment of water-soluble inorganic ions in $PM_{2.5}$ during haze days in Beijing urban area. *J. Capital Normal Univ. (Nat. Sci. Ed.)* **2017**, *38*, 49−57.
(36) Jia, Y. Q.; Yin, H. M.; Zhou, R.; Yu, Y.; Cao, G.; Xie, H. Characteristics of water-soluble inorganic ions and inorganic elements of $PM_{2.5}$ in Beijing. *Environ. Chem.* **2018**, *37*, 2767−2773.
(37) Yan, Z. W.; Pei, L.; Zhou, T. J.; Zhu, J. Unusually clear sky in Beijing during winter 2017 and the underlying large-scale climatic anomalies: With implication for "haze-climate" study. *Acta Meteorol. Sin.* **2018**, *76*, 816−823.
(38) Jia, J.; Han, L. H.; Cheng, S. Y.; Zhang, H. Y.; Lv, Z. Pollution characteristic of $PM_{2.5}$ and secondary inorganic ions in Beijing-Tianjin-Hebei region. *China Environ. Sci.* **2018**, *38*, 801−811.
(39) Zhang, Y.; Huang, W.; Cai, T. Q.; Fang, D. Q.; Wang, Y. Q.; Song, J.; Hu, M.; Zhang, Y. Concentrations and chemical compositions of fine particles ($PM_{2.5}$) during haze and non-haze days in Beijing. *Atmos. Res.* **2016**, *174*−*175*, 62−69.
(40) Sun, J. Y.; Zhang, L.; Shen, X. J.; Che, H. C.; Zhang, Y. M.; Fan, R. X. A review of the effects of relative humidity on aerosol scattering properties. *Acta Meteorol. Sin.* **2016**, *74*, 672−682.
(41) Zhang, Z. Z.; Li, H.; Liu, H. Y.; Ni, R. X.; Li, J. J.; Deng, L. Q.; Lu, D.; Cheng, X.; Duan, P.; Li, W. A preliminary analysis of the surface chemistry of atmospheric aerosol particles in a typical urban area of Beijing. *J. Environ. Sci.* **2016**, *47*, 71−81.

https://doi.org/10.1021/acsomega.2c02919
ACS Omega 2022, 7, 35575−35585